We are IntechOpen,
the world's leading publisher of
Open Access books
Built by scientists, for scientists

4,800
Open access books available

122,000
International authors and editors

135M
Downloads

Our authors are among the

154
Countries delivered to

TOP 1%
most cited scientists

12.2%
Contributors from top 500 universities

CLARIVATE ANALYTICS
BOOK CITATION INDEX
INDEXED

WEB OF SCIENCE™

Selection of our books indexed in the Book Citation Index
in Web of Science™ Core Collection (BKCI)

Interested in publishing with us?
Contact book.department@intechopen.com

Numbers displayed above are based on latest data collected.
For more information visit www.intechopen.com

Microstrip Antenna Arrays

Dr. Albert Sabban
Ort Braude College, Karmiel
Israel

1. Introduction

Microstrip antennas posse's attractive features such as low profile, flexible, light weight, small volume and low production cost. In addition, the benefit of a compact low cost feed network is attained by integrating the RF feed network with the radiating elements on the same substrate. Microstrip antennas are widely presented in books and papers in the last decade (J.R James et al, 1981; A. Sabban, 1981; A. Sabban,1983; A. Sabban & E. Navon, 1983). Microstrip antennas maybe employed in communication links, seekers and in biomedical systems.

In this chapter we present several applications of microstrip antennas. The design of mm wave microstrip antenna arrays with high efficiency is presented in this chapter. Gain limitation in microstrip antenna arrays due to losses in the feed network are presented by (J.R James et. al., 1981). However, this discussion is limited to a 12GHz plane slot array and radiation and dielectric losses are neglected.

The efficiency of microstrip antenna arrays may be improved significantly by reducing losses in the feed network. Losses in the microstrip feed network are due to conductor loss, radiation loss and dielectric loss. Equations to calculate conductor loss and dielectric loss in microstrip lines are given by (J.R James et. al., 1981). In (A. Sabban & K.C. Gupta, 1991; A. Sabban, 1991) a planar multiport network modeling approach has been used to evaluate radiation loss from microstrip discontinuities. Full-wave analysis has been used by (P.B. Kathei & N.G. Alexopoulos, 1985) to calculate radiation conductance of an open-circuited microstrip line. Full-wave analysis methods and software are available for characterization of microstrip discontinuities. These analyses include radiation effects also. The power radiated from a discontinuity may be evaluated from the computed S parameters. However, evaluation of power radiated from the computed S parameters requires a high numerical accuracy of the computed results. Therefore radiation loss values based on full-wave analysis are not widely available.

In this chapter losses in 64 and 256 patch antenna array at Ka band are evaluated. Methods to minimize these losses and to improve the antenna efficiency are presented.

In the literature several applications of mm wave microstrip antenna arrays are described. Gain limitation in microstrip antenna arrays may be solved by employing active microstrip arrays.

However, active microstrip arrays have several disadvantages such as significantly increase in power consumption, weight and dimensions. In some applications reflect arrays are employed. In reflect arrays the received power is transmitted by the same antenna array. Efficiency of microstrip antenna arrays may be improved by using a waveguide feed

network. However, this result in significantly increase in the antenna weight and dimensions. In this case a transition from microstrip to waveguide is required.

Several imaging approaches are presented (M.M. Milkov, 2000; G de Lange et. Al., 1999; A. Rahman et. al., 1996; A. Luukanen et. al., 2001; M. D. Jack et. al., 2001; G. N. Sinclair et. al., 2000). The common approach is based on an array of radiators (antennas) that receives radiation from a specific direction by using a combination of electronic and mechanical scanning. Another approach is based on a steering array of radiation sensors at the focal plane of a lens of reflector. The sensor can be an antenna coupled to a resistor. In this chapter we present the development of millimeter wave radiation detection array. The detection array may employ around 256 to 1024 patch antennas. These patches are coupled to a resistor. Optimization of the antenna structure, feed network dimensions and resistor structure allow us to maximize the power rate dissipated on the resistor. Design considerations of the detection antenna array are given in this chapter.

Microstrip and printed antennas features make them excellent candidates to serve as antennas in biomedical systems. However, the electrical performance of the antenna is altered significantly in vicinity to human body. These facts complicate significantly the antenna design. The electrical performance of a new class of wideband wearable printed antennas for medical applications is presented in this Chapter. RF transmission properties of human tissues have been investigated in several papers (C. Lawrence et. al., 2003; D. Werber et. al., 2006). However, the effect of human body on the electrical performance of the antennas at frequencies that biomedical system operates is not presented. The interaction between microstrip antennas and human body is presented in this Chapter. The antenna bandwidth is around 10% for VSWR better than 2:1. The antenna beam width is around 100°. The antenna gain is around 4dBi. If the air spacing between the sensors and the human body is increased from 0mm to 5mm the antenna resonant frequency is shifted by 5%.

2. Microstrip antenna arrays with high efficiency

One of the major advantages of microstrip antennas is the simplicity of array construction (J.R James et. al., 1981). The radiating elements may be etched jointly with the feed network as an integrated structure leading to a very compact and low cost design. Although the technique for designing feed networks is well established, several difficulties are encountered while implementing it at mm wave frequencies. Microstrip line losses increase considerably at mm wave frequencies. Conductor, dielectric and radiation losses are the major components of loss in mm-wave microstrip antenna arrays. At frequencies ranging from 30 to 40 GHz, conductor losses are around 0.15 to 0.2 dB per wavelength, dielectric losses are around 0.045 dB per wavelength for a 50Ω line on a 10 mil substrate with εr=2.2.

The open nature of microstrip configuration suffers from radiation. In mm-wave microstrip antenna arrays, more bends, T-junctions and other discontinuities are introduced in the feed network and radiation loss increases considerably. The multiport network model is employed to evaluate radiation loss from microstrip discontinuities. Minimization of losses in the microstrip feed network may results in microstrip antenna arrays with high efficiency.

2.1 Evaluation of microstrip feed network losses

Equations to calculate conductor loss and dielectric loss in microstrip lines are given in (J.R James et. al., 1981). Dielectric loss is incorporated in the multiport network analysis by considering a complex dielectric constant. Conductor losses are included in the analysis by

defining an equivalent loss tangent δc, given by δc=√ 2/ωμσ/h, where σ is the strip conductivity, h is the substrate height and μ is the free space permeability.

2.1.1 Evaluation of radiation loss

The multiport network model is employed to evaluate radiation loss from microstrip feed networks by adding a number of open ports at the edges of the planar model for the discontinuity structure. The multiport network model is based on the parallel-plate wave-guide model (G. Compa & Mehran, 1975) for microstrip lines. A similar network modeling approach has been used for analysis of microstrip discontinuities (A. Sabban & K.C. Gupta, 1991). The planar waveguide model consists of two parallel conductors bounded by magnetic walls in the transverse directions. In this modeling approach for microstrip structures, fields underneath the microstrip configuration, the external fields (radiated fields, surface waves) are modeled separately in terms of multiport sub networks by adding an equivalent edge admittance network connected to the edges of the microstrip configuration. These sub networks are characterized in terms of Z-matrices that are evaluated by using the Green's function approach. The sub-networks are combined using the segmentation technique to obtain circuit characteristics such as scattering parameters. Equations to compute the sub-networks Z-matrices are given in (A. Sabban, 1991).

The multiport network model is used to evaluate the voltage distributions at the open ports, voltages at the discontinuity edges are represented by equivalent magnetic current sources, as shown in Fig.1. The amplitude M of the magnetic current elements is twice that of the edge voltage at that location and the phase of the magnetic current is equal to the phase of the corresponding voltage. The total radiation is computed using the superposition of the far-field radiated by each section. Referring to the coordinate system, shown in Fig. 2, the far-field pattern $F(\theta,\phi)$ may be written in terms of voltages at the various elements. With the voltage at the ith element as ($V(i)\,e^{i\alpha(i)}$), we have

$$F(\theta,\phi) = \sum_{i=1}^{N} 2V(i)W(i)\exp\{k_0\gamma_0(i) + \alpha(i)\}F_i(\theta,\phi) \tag{1}$$

where

$$F_i(\theta,\phi) = \frac{\sin(\dfrac{k_0W(i)}{2}\cos\theta)}{\dfrac{k_0W(i)}{2}\cos\theta}\sin\theta$$

$$\gamma_0(i) = X_0(i)\sin\theta\cos\phi + Y_0(i)\cos\theta$$

and N is the number of ports , $X_0(i)$, $Y_0(i)$ specify the location of the ith magnetic current element, k_0 is the free space wave number, $W(i)$ is the width of the ith element. The factor 2 in (1) accounts for the image of the magnetic current with respect to the ground plane. The radiated power is calculated by the integration of the Poynting vector over the half space and may be written as

$$P_r = \frac{1}{240\pi}\int_{\frac{-\pi}{2}}^{\frac{\pi}{2}}\int_{0}^{\pi}(|E_\theta|^2 + |E_\phi|^2)r^2\sin\theta \; d\theta \; d\phi \tag{2}$$

The fields E_θ and E_ϕ are expressed in terms of $F(\theta,\phi)$ as

$$E_\theta = \overset{\wedge}{a_\theta}(\frac{-jk_0}{4\pi r}F(\theta,\phi)F_\theta) \tag{3}$$

$$E_\phi = \overset{\wedge}{a_\varphi}(\frac{-jk_0}{4\pi r}F(\theta,\phi)F_\phi) \tag{4}$$

where

$$F_\phi = \sin\phi'\sin\phi + \cos\delta\cos\phi\cos\phi' \tag{5}$$

$$F_\theta = -\sin\phi'\cos\theta\cos\phi + \cos\delta\cos\theta\sin\phi + \sin\delta\cos\phi'\sin\theta \tag{6}$$

$$\cos\theta' = \sin\theta\sin\phi\sin\delta + \cos\theta\cos\delta \tag{7}$$

$$\cos\phi' = \sin\theta\cos\phi / \sqrt{1-\cos^2\theta'} \tag{8}$$

The radiated power may be expressed as a fraction of input power $10\log_{10}(P_r/P_i)$ dB. The radiation loss may be expressed as, Radiation Loss (dB) = $10\log_{10}(1-P_r/P_i)$. Where P_i is the input power at port 1. P_i is calculated from input current and the input impedance of the discontinuity terminated in matched loads at other ports.

2.1.2 Radiation loss from microstrip discontinuities

Computation of microstrip feed network losses are given in (A. Sabban, 1991). As an example radiation loss of a right angle bend in a 50 ohm line on a 10 mil duroid substrate with εr=2.2, is 0.1dB at 30GHz and 0.17 dB at 40GHz. Dielectric loss can be reduced by using substrates with a low dielectric loss. To minimize radiation loss, the number of discontinuities, such as bends and T-Junctions, should be made as small as possible. Radiation from a curved microstrip line is much smaller compared to radiation from right angled bend. Moreover in order to reduce radiation loss in the feed network, the width of the microstrip line is designed to be less than 0.12λ on 0.25mm substrate with εr=2.2.

Conductor loss may be minimized by designing the feed network length per wavelength as short as possible. By using a multilayer feed network design, the feed network length per wavelength is minimized considerably. Gold plating of the microstrip lines decreases conductor losses. Low loss coaxial cables may replace in the microstrip feed network long sections of microstrip lines. As an example the insertion loss of a flexible cable at 30GHz is 0.039 dB per centimeter. However, the insertion loss at 30GHz of a 50 ohm microstrip line on a 10 mil substrate with εr=2.2 is around 0.2dB. By replacing a microstrip line with length of ten centimeters with a coaxial transmission line, the loss decreases by 1.6 dB. The coaxial line may be an integral part of the feed network or it may be embedded in the metallic ground plane. The transition from microstrip line to coaxial line is straightforward. The coaxial line center conductor is soldered to the microstrip line and the outer conductor is soldered or glued to the ground plane, by using conductive glue.

2.2 64 and 256 microstrip antenna arrays with high efficiency

Microstrip antenna arrays with integral feed networks may be broadly divided into arrays fed by parallel feeds and series fed arrays. Usually series fed arrays are more efficient than

parallel fed arrays. However, parallel fed arrays have a well controlled aperture distribution.

Two Ka band microstrip antenna arrays which consist of 64 radiating elements have been designed. The first array uses a parallel feed network and the second uses a parallel-series feed network as shown in Fig. 3.a and 3.b. Comparison of the performance of the arrays is given in Table 1. Results given in Table 1 verifies that the parallel series fed array is more efficient than the parallel fed array due to minimization of the number of discontinuities in the parallel series feed network.

The parallel-series fed array has been modified by using a five centimeter coaxial line to replace the same length of microstrip line. Results given in Table 1 indicates that the efficiency of the parallel series fed array that incorporates coaxial line in the feed network is around 67.6% due to minimization of the microstrip line length.

PARAMETER	Corporate feed	Parallel feed	Microstrp & coaxial corporate feed
Number of elements	64	64	64
Beamwidth(deg.)	8.5	8.5	8.5
Computed gain(dBi)	26.3	26.3	26.3
Microstrip line loss(dB)	1.1	1.2	0.5
Radiation loss T-J.(dB)	0.27	0. 45	0.27
Radiation loss bends(dB)	0.4	0.8	0.4
Radiation loss steps(dB)	0.045	-	0.045
Mismatch Loss (dB)	0.5	0.5	0.5
Expected Gain(dBi)	24.0	23.35	24.6
Efficiency (%)	58.9	50.7	67.6

Table 1. Performance of 64 Elements Microstrip Antenna arrays

Two microstrip antenna arrays which consist of 256 radiating elements has been designed. In the first array, Type A as shown in Fig. 4.a, the number of microstrip discontinuities is minimized. The second array, Type B as shown in Fig. 4.b, incorporate more bend discontinuities in the feeding network. Comparison of the performance of the arrays is given in Table 2. The Type (A) array with 256 radiating elements has been modified by using a ten

PARAMETER	Type A	Type B	Type A& Microstrp coaxial feed
Number of elements	256	256	256
Beamwidth(deg.)	4.2	4.2	4.2
Computed gain(dBi)	32	32	32
Microstrip line loss(dB)	3.1	3.1	1.5
Radiation loss T-J.(dB)	0.72	0.72	0.72
Radiation loss bends(dB)	0.13	1.17	0.13
Radiation loss steps(dB)	0.12	-	0.12
Mismatch Loss (dB)	0.5	0.5	0.5
Expected Gain(dBi)	27.43	26.5	29.03
Efficiency (%)	34.9	28.2	50.47

Table 2. Performance of 256 Elements Microstrip Antenna arrays
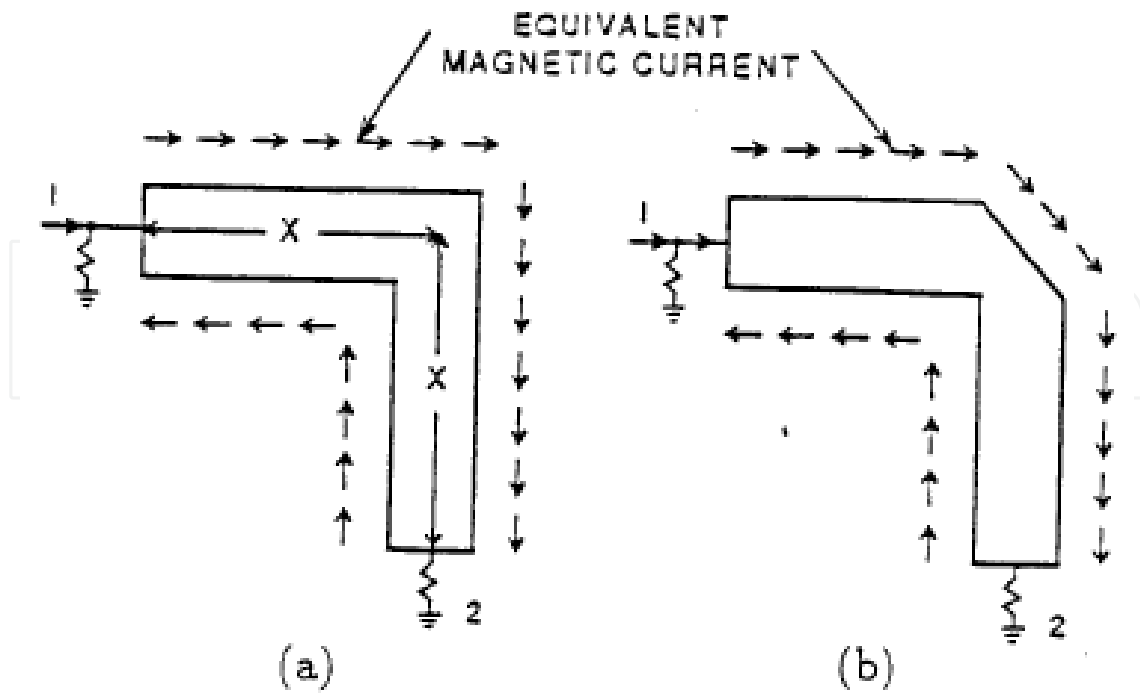
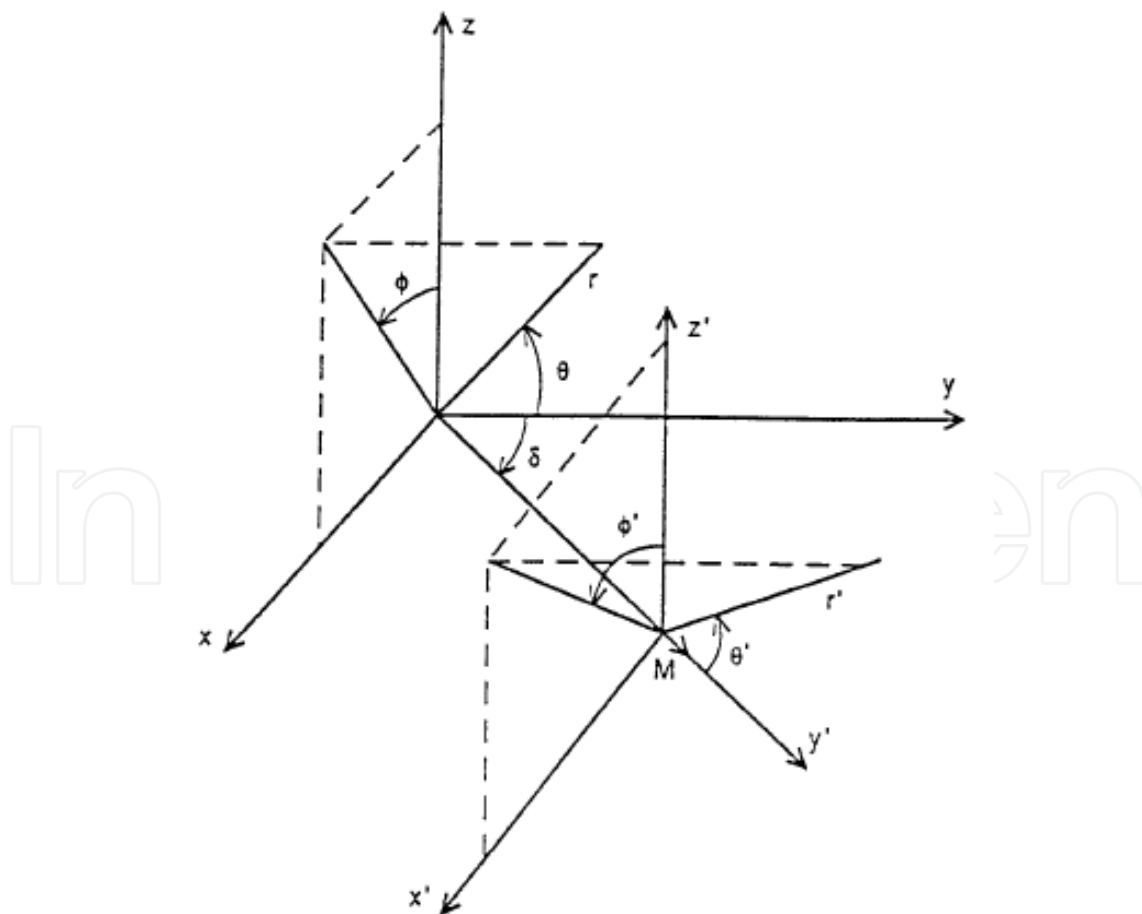Fig. 1. Equivalent magnetic current distribution at discontinuity edges

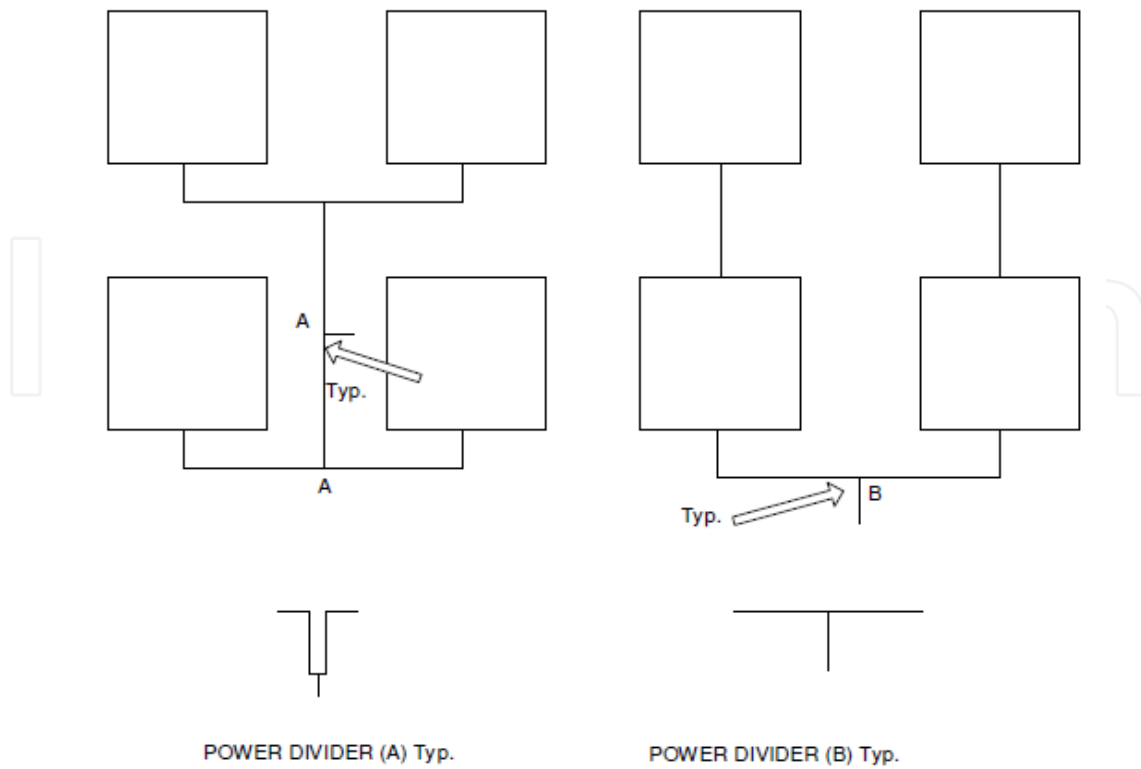Fig. 2. Coordinate system for external field calculations.

Fig. 3. Configuration of 64 elements microstrip antenna array
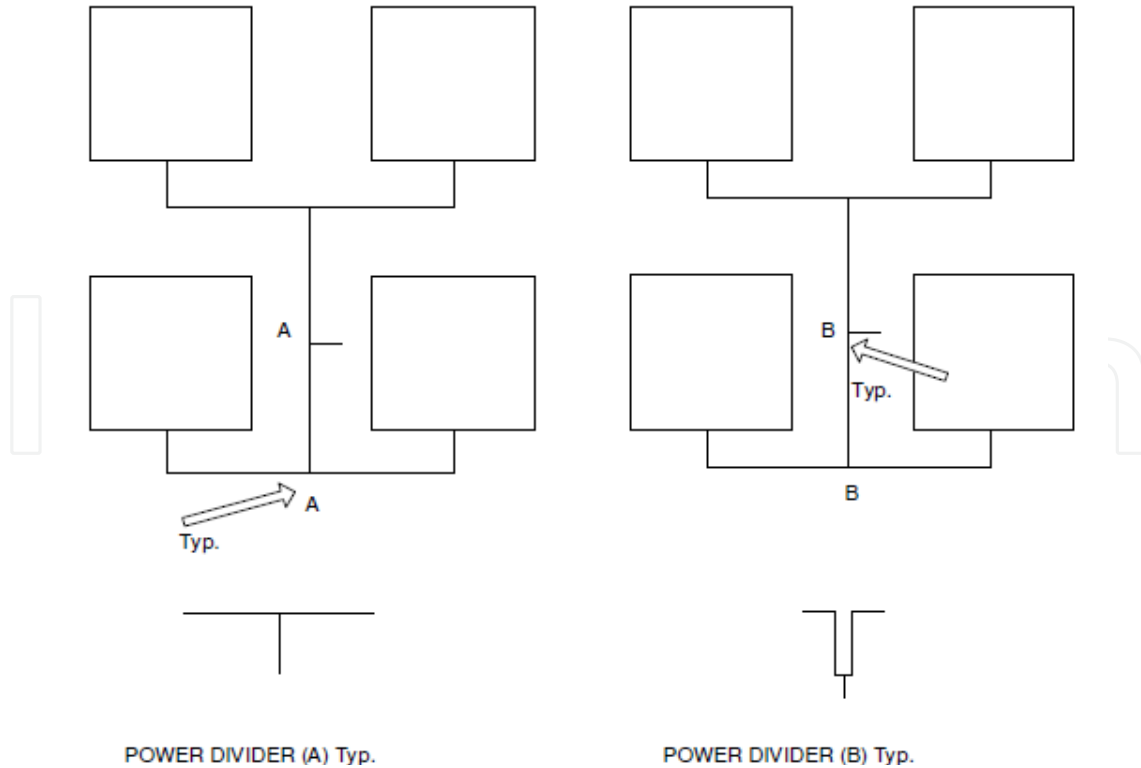a. Parallel feed network. b. Parallel series feed network.

Fig. 4. Configuration of 256 elements microstrip antenna array
a. Array type A. b. Array type B.

centimeter coaxial line to replace the same length of microstrip line. Comparison of the arrays performance is given in Table 2. Table 2 shows that the gain of the modified array has been increased by 1.6 dB.

Results given in Table 2 verifies that the Type A array is more efficient than the Type B array due to minimization of the number of bend discontinuities in the Type A array feed network. The measured gain results are very close to the computed gain results and verify the loss computation presented in this chapter.

3. W band microstrip antenna detection array

Losses in the microstrip feed network are very high in the W band frequency range. In W band frequencies we may design a detection array. The array concept is based on an antenna coupled to a resistor. A direct antenna-coupling surface to a micro machined micro bridge resistor is used for heating and sensing. Analog CMOS readout circuit may be employed as a sensing channel per pixel. Fig. 5 presents a pixel block diagram.
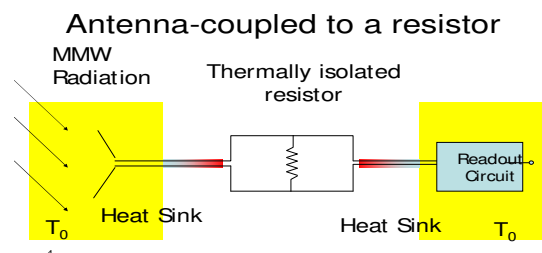
Fig. 5. Antenna coupled to a resistor

3.1 The array principle of operation

The antenna receives effective mm wave radiation. The radiation power is transmitted to a thermally isolated resistor coupled to a Ti resistor. The electrical power raises the structure temperature with a short response time. The same resistor changes its temperature and therefore its electrical resistance. Fig. 6 shows a single array pixel. The pixel consist a patch antenna, a matching network, printed resistor and DC pads. The printed resistor consist Titanium lines, a Titanium resistor coupled to an isolated resistor.
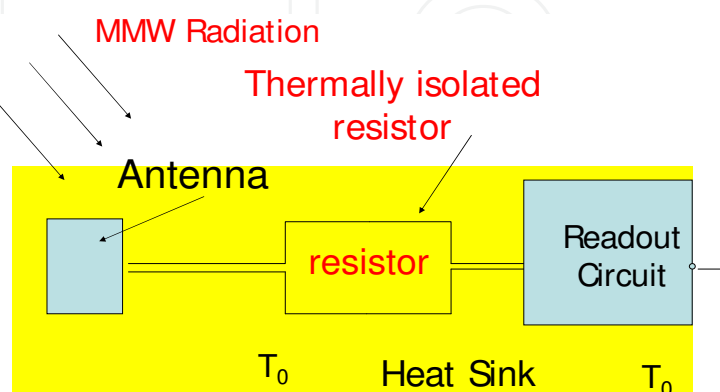
Fig. 6. A single array pixel

The operating frequency range of 92 to 100GHz is the best choice. In the frequency range of 30-150GHz there is a proven contrast between land, sky and high transmittance of clothes.

Size and resolution considerations promote higher frequencies above 100GHz. Typical penetration of clothing at 100GHz is 1dB and 5 to 10dB at 1THz. Characterization and measurement considerations promote lower frequencies. The frequency range of 100 GHz allows sufficient bandwidth when working with illumination. The frequency range of 100 GHz is the best compromise. Fig. 7 presents the array concept. Several types of printed antennas may be employed as the array element such as bowtie dipole, patch antenna and ring resonant slot.

3.2 W band antenna design

The bowtie dipole and a patch antenna have been considered as the array element. Computed results shows that the directivity of the bowtie dipole is around 5.3dBi and the directivity of a patch antenna is around 4.8dBi. However the length of the bowtie dipole is around 1.5mm the size of the patch antenna is around 700x700µm. We used a quartz substrate with thickness of 250µm. The bandwidth of the bowtie dipole is wider than that of a patch antenna. However, the patch antenna bandwidth meets the detection array electrical specifications. We chose the patch antenna as the array element since the patch size is significantly smaller than that of the bowtie dipole. This feature allows us to design an array with a higher number of radiating elements. The resolution of detection array with a higher number of radiating elements is improved. We also realized that the matching network between the antenna and the resistor has smaller size for a patch antenna than that for a bowtie dipole. The matching network between the antenna and the resistor consist of microstrip open stubs. Fig. 8 shows the 3D radiation pattern of the Bowtie dipole. Fig. 9 presents S11 parameter of the patch antenna. We compared the electrical performance of the antennas.
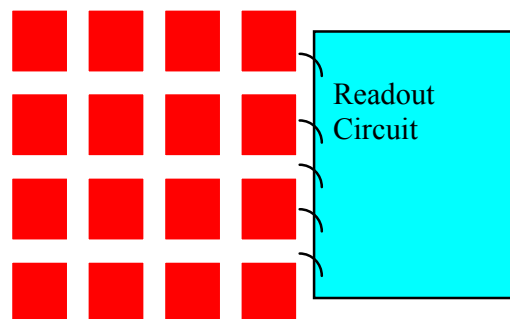
Fig. 7. Array concept
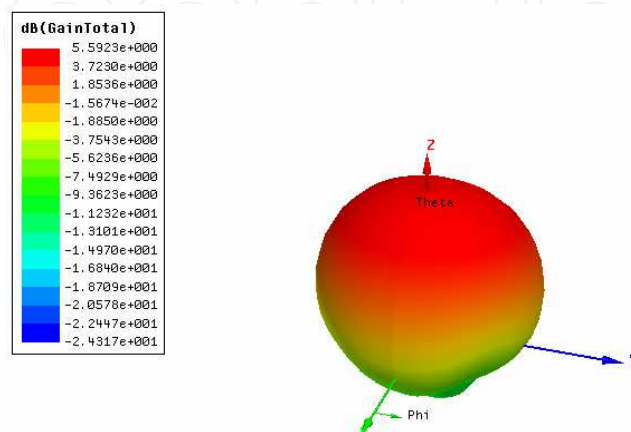
Fig. 8. Dipole 3D radiation pattern

Fig. 7 shows the 3D radiation pattern of the patch antenna.
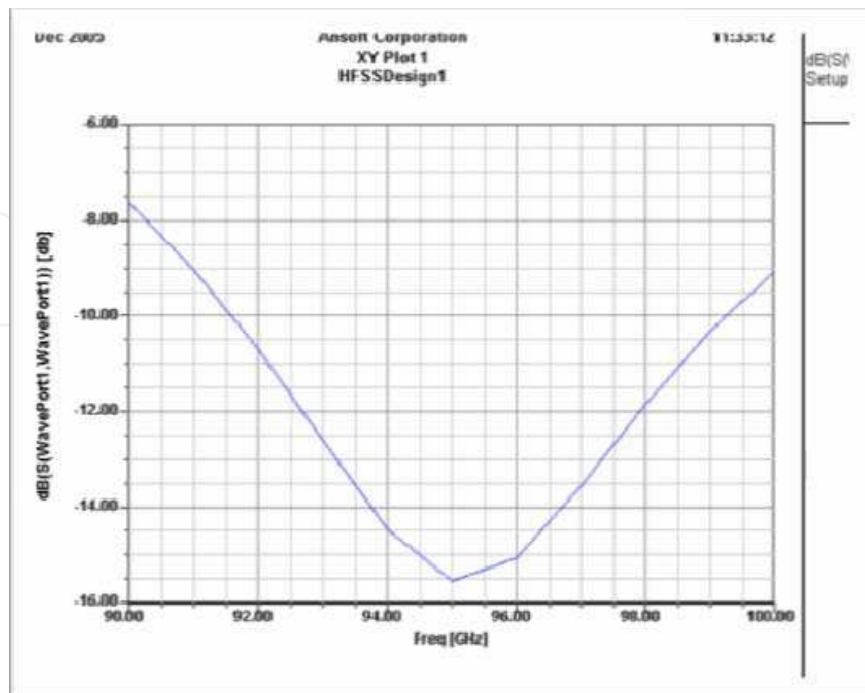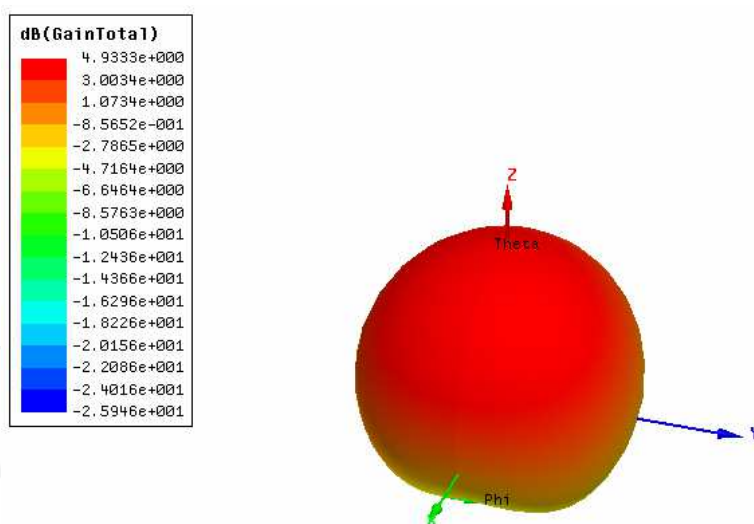

Fig. 9. Patch S11 computed results

Fig. 10. Patch 3D radiation pattern

3.3 Resistor design

As described by (M.M. Milkov, 2000) the resistor is thermally isolated from the patch antenna by using a sacrificial layer. Optimizations of the resistor structure maximize the power rate dissipated on the resistor. Ansoft HFSS software is employed to optimize the height of the sacrificial layer, the transmission line width and length. Dissipated power on Titanium resistor is higher than the dissipated power on Platinum resistor. The rate of the dissipated power on the resistor is around 25%. Material properties are given in Table 3.

Ti	siNi	Units	Property
7	1.6	W/m/K	Conductivity [K]
520	770	J/Kg/K	Capacity [C]
4.5	2.85	Gr/cm^3	Density [ρ]
90	>1e8	Ω/□	Resistance
0.1	**0.1**	**µm**	**Thickness**

Table 3. Material properties

The sacrificial layer thickness may be 2 to 3µm. Fig. 11 shows the resistor configuration.
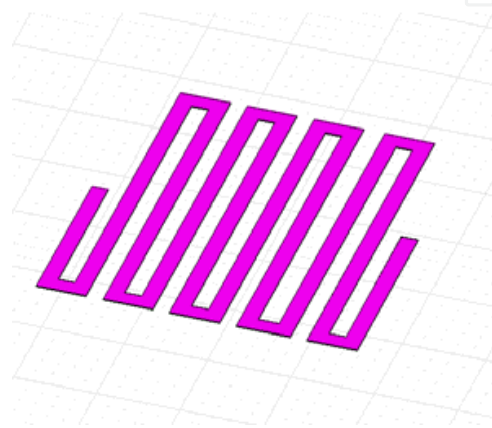
Fig. 11. Resistor Configuration

3.4. 220GHz microstrip patch antenna

Quartz substrate with thickness of 50µm to 100µm has been used to fabricate microstrip antennas at frequencies higher than 200GHz. The size of the patch antenna is around 300x300µm.

Fig. 12 presents S11 parameter of the patch antenna. Fig. 13 shows the 3D radiation pattern of the patch antenna.
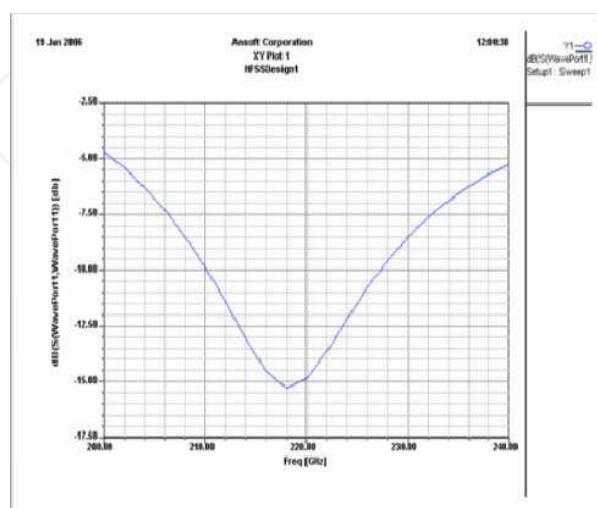
Fig. 12. 220GHz Patch S11 computed results
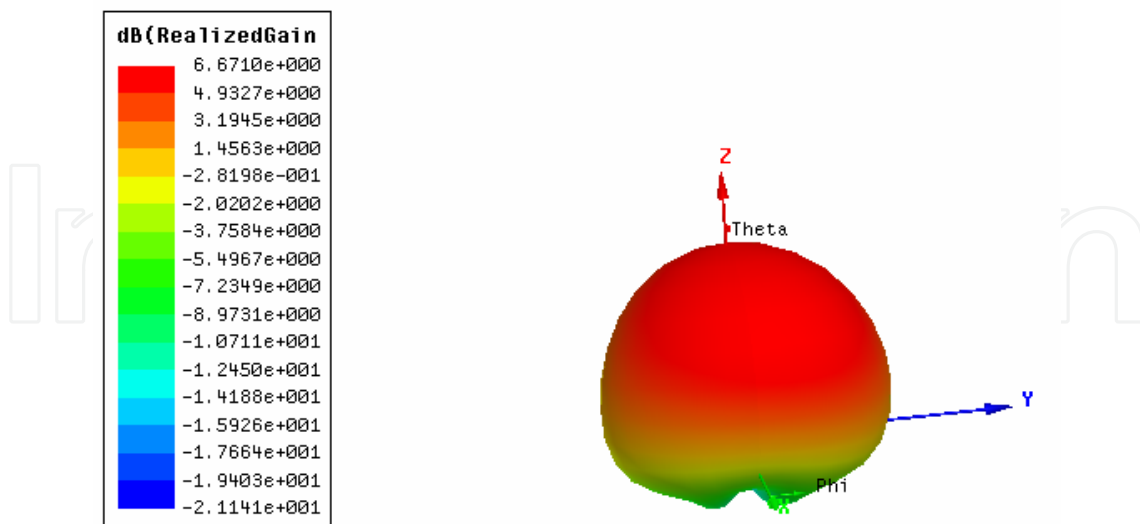
Fig. 13. 220GHz Patch 3D radiation pattern

4. Medical applications of microstrip antennas

Microstrip antennas posse's attractive features such as low profile, flexible, light weight, small volume and low production cost. Microstrip and printed antennas features make them excellent candidates to serve as antennas in biomedical systems. However, the antenna electrical performance is altered significantly in vicinity to human body. These facts complicate significantly the antenna design. The electrical performance of a new class of wideband wearable printed antennas for medical applications is presented in this Chapter. RF transmission properties of human tissues have been investigated in several papers (C. Lawrence et. al., 2003; D. Werber et. al., 2006). However, the effect of human body on the electrical performance of the antennas at frequencies that biomedical system operates is not presented. A new class of wideband compact wearable printed and microstrip antennas for medical applications is presented in this chapter.

4.1 Dual polarized 434MHz printed antenna

A new compact microstrip loaded dipole antennas has been designed to provide horizontal polarization. The antenna consists of two layers. The first layer consists of RO3035 0.8mm dielectric substrate. The second layer consists of RT-Duroid 5880 0.8mm dielectric substrate. The substrate thickness determines the antenna bandwidth. However, with thinner substrate we may achieve better flexibility. We also designed a thicker double layers microstrip loaded dipole antennas with wider bandwidth. A printed slot antenna provides a vertical polarization. The proposed antenna is dual polarized. The printed dipole and the slot antenna provide dual orthogonal polarizations.

The dual polarized antenna is shown in Fig. 14. The antenna dimensions are 26x6x0.16 cm. The antenna may be employed as a wearable antenna on a human body. The antenna may be attached to the patient shirt in the patient stomach zone. Alternatively the antenna may

be attached to the patient back. The antenna has been analyzed by using Agilent ADS software. There is a good agreement between measured and computed results. The antenna bandwidth is around 10% for VSWR better than 2:1 as shown in Fig. 15. The antenna beam width is around 100°. The antenna gain is around 4dBi.
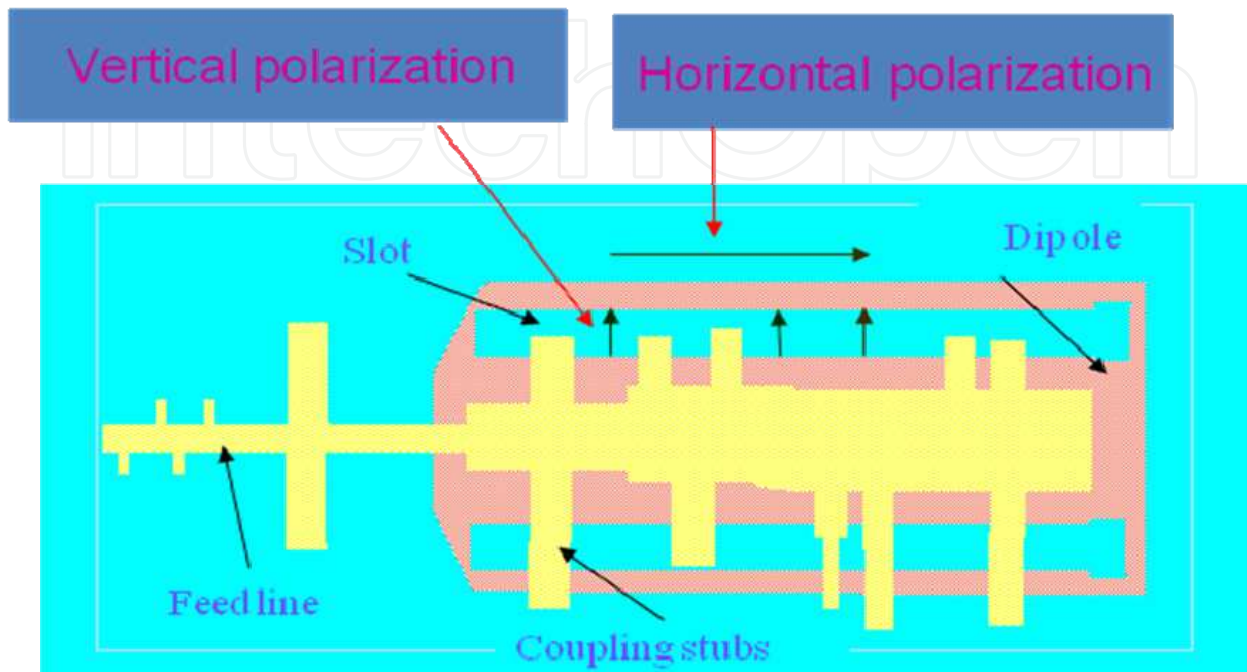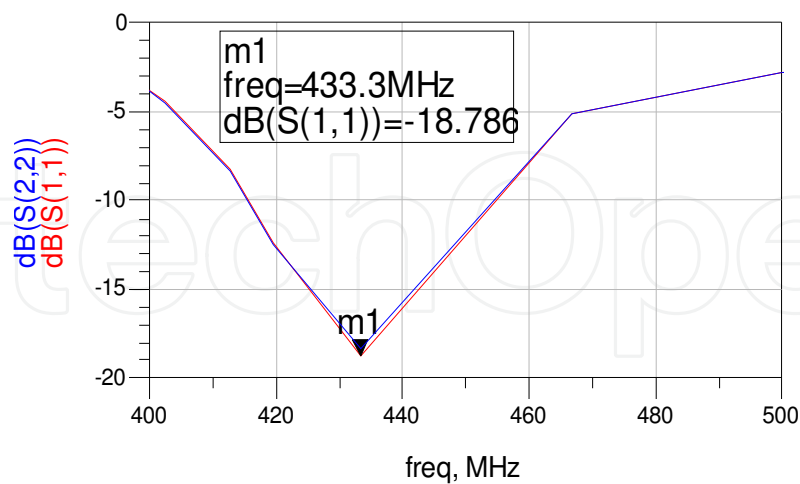

Fig. 14. Printed dual polarized antenna

Fig. 15. Computed S11 and S22 results

The computed S11 and S22 parameters are presented in Fig. 15. Fig. 16 presents the antenna measured S11 parameters. The computed radiation pattern is shown in Fig. 17. The antenna cross-polarized field strength may be adjusted by varying the slot feed location.
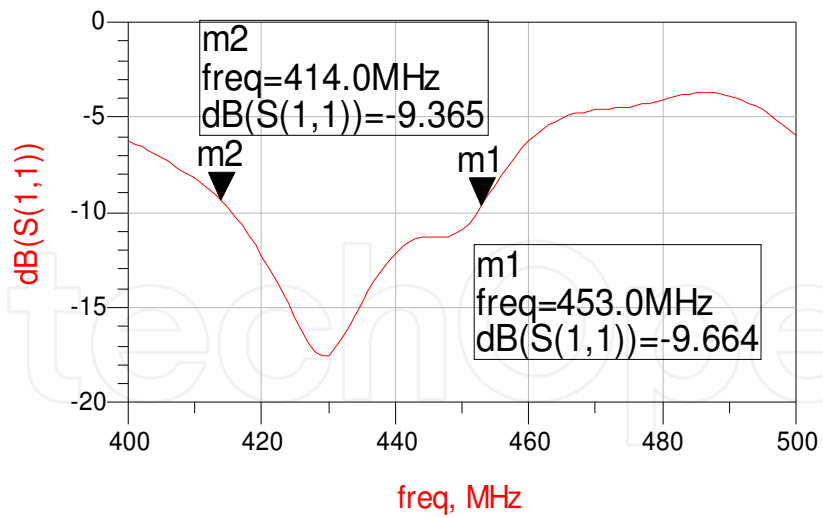
Fig. 16. Measured S11 on human body
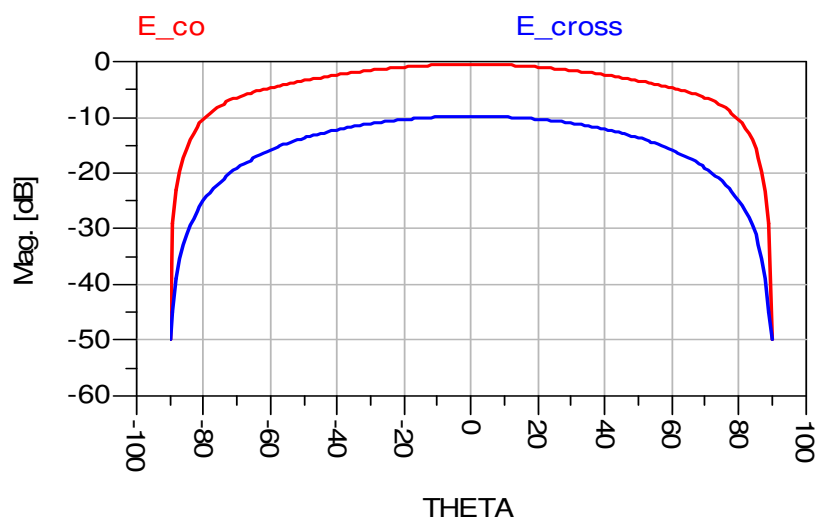
Fig. 17. Antenna Radiation pattern

The antenna dimensions may be reduced to 6X6X0.16cm by employing a folded antenna configuration as shown in Fig. 18.
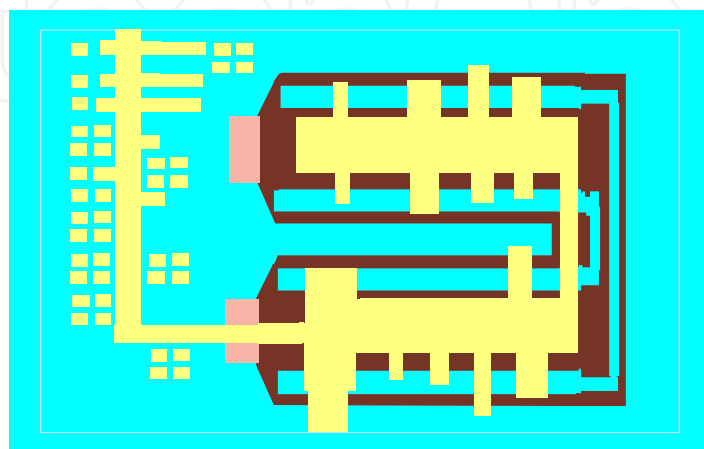
Fig. 18. Folded dual polarized antenna

Fig. 19 presents the antenna computed S11 and S22 parameters. The computed radiation pattern of the folded dipole is shown in Fig. 20.
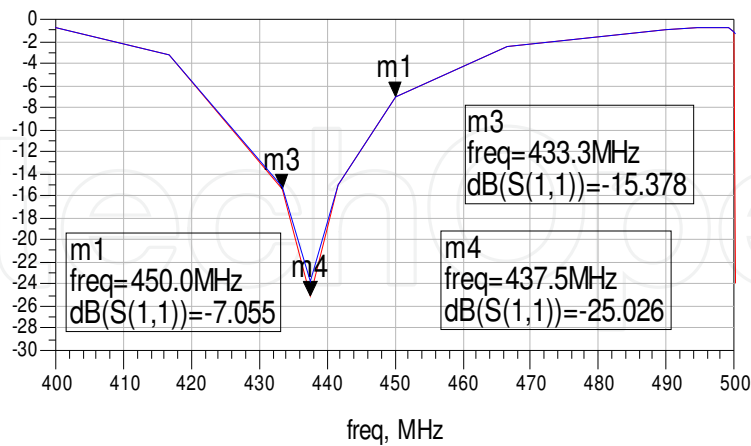
Fig. 19. Folded antenna Computed S11 and S22 results
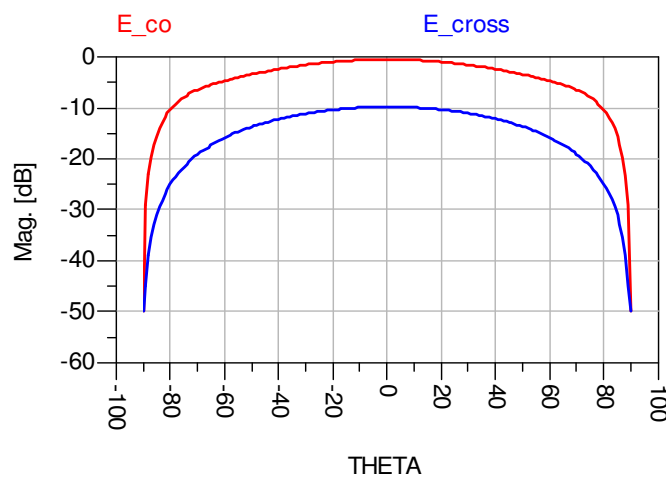
Fig. 20. Folded antenna Radiation pattern

4.2 New loop antenna with ground plane

A new loop antenna with ground plane has been designed on Kapton substrates with thickness of 0.25mm and 0.4mm. The loop antenna diameter is around 50mm. The antenna is shown in Fig. 21. Fig. 22 presents the Loop antenna computed S11 on human body. The computed radiation pattern is shown in Fig 23.

Table 4 compares the electrical performance of a loop antenna with ground plane with a loop antenna without ground plane. There is a good agreement between measured and computed results of antenna parameters on human body.

VSWR	Gain dBi	Beam width 3dB	Antenna
4:1	0	100°	Loop no GND
2:1	0	100°	Loop with GND

Table 4. Comparison of Loop Antennas
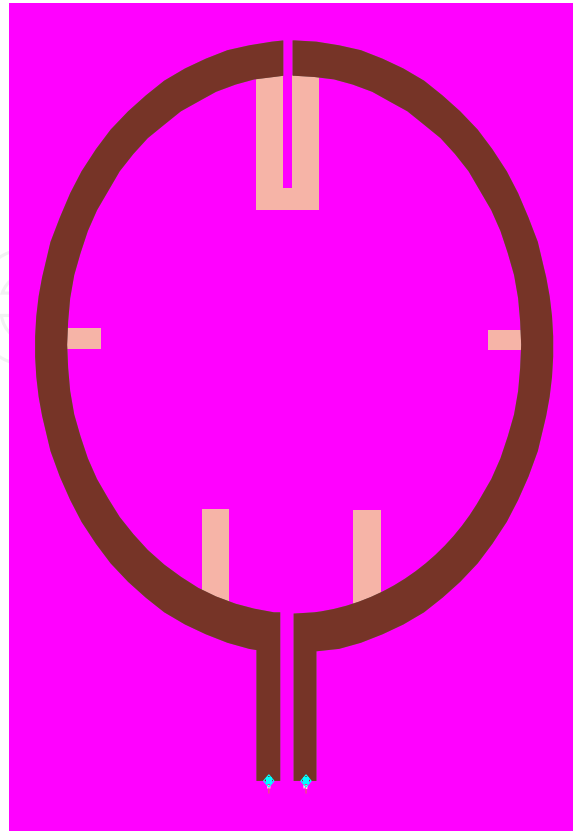
Fig. 21. Loop antenna with ground plane
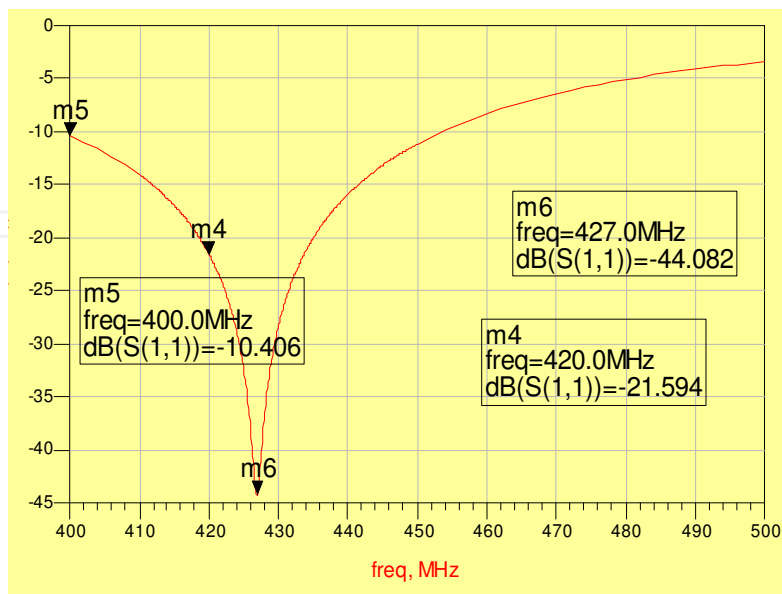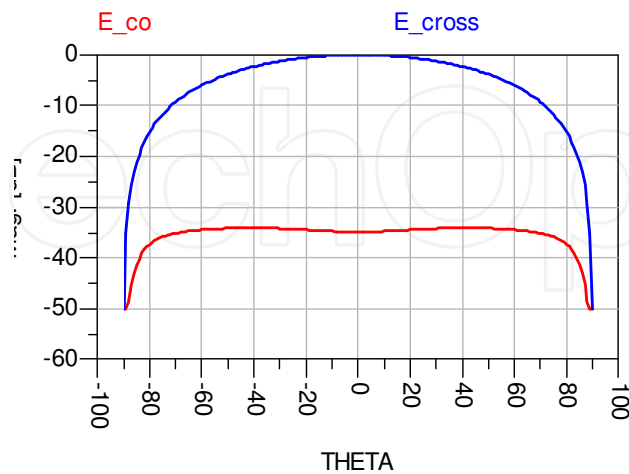

Fig. 22. Computed S11 of Loop Antenna

Fig. 23. Loop Antenna Radiation pattern on human body

4.3 Antenna S11 variation as function of distance from body

The Antenna input impedance variation as function of distance from the body has been computed by employing ADS software. The analyzed structure is presented in Fig. 24.
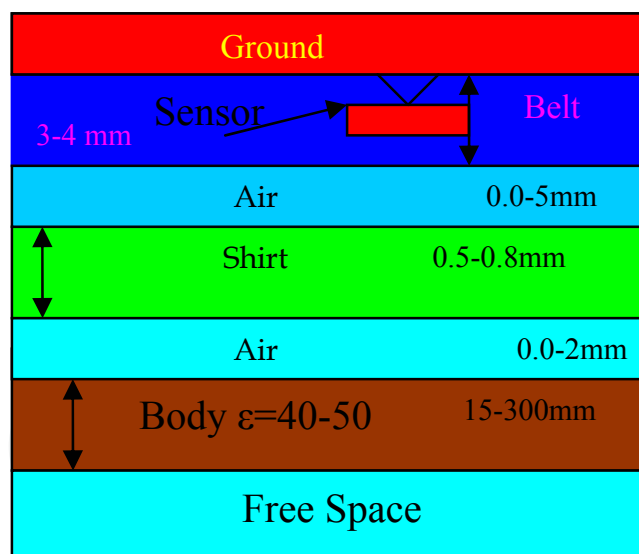

Fig. 24. Analyzed structure for Impedance calculations

Properties of human body tissues are listed in Table 5 see (C. Lawrence et. al., 2003).
These properties were employed in the antenna design. Fig. 25 presents S11 results for different belt thickness, shirt thickness and air spacing between the antennas and human body. One may conclude from results shown in Fig. 26 that the antenna has V.S.W.R better than 2.5:1 for air spacing up to 8mm between the antennas and patient body. For frequencies ranging from 415MHz to 445MHz the antenna is matched when there is no air spacing between the antenna and the patient body.
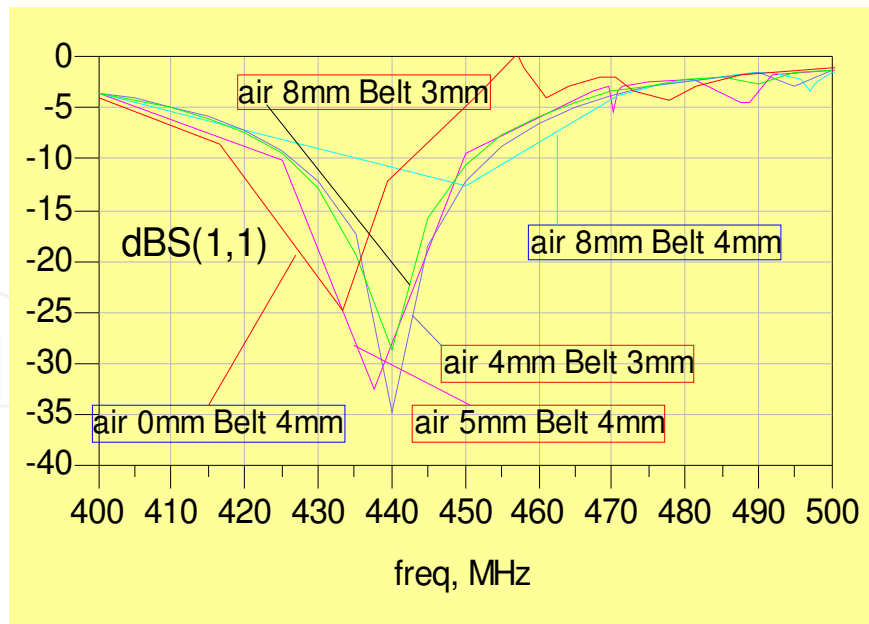
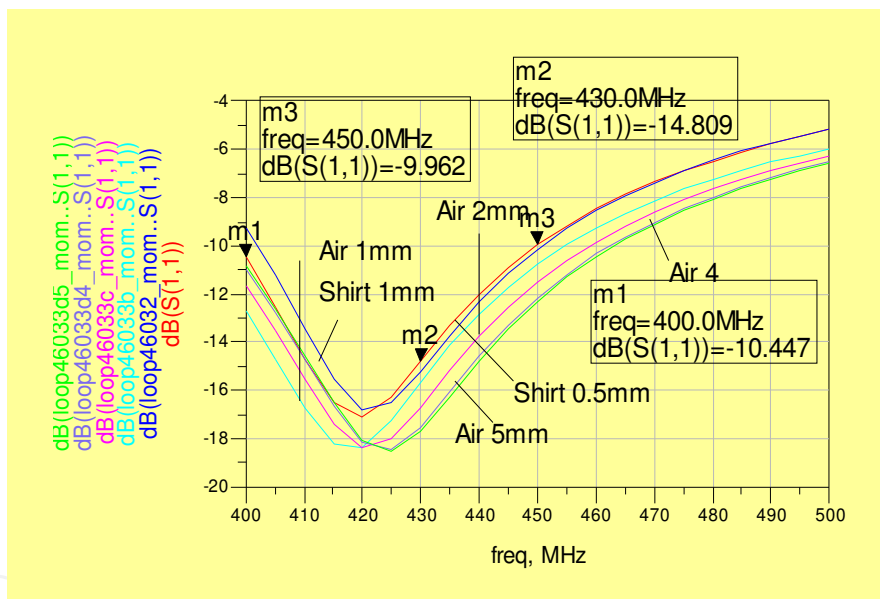Fig. 25. S11 results for different antenna position relative to the human body

Fig. 26. Folded antenna S11 results for different position relative to the human body

600 MHz	434 MHz	Property	Tissue
0.6	0.57	σ	Skin
40.43	41.6	ε	
0.73	0.67	σ	Stomach
41.41	42.9	ε	
1.06	0.98	σ	Colon, Muscle
61.9	63.6	ε	
0.27	0.27	σ	Lung
38.4	38.4	ε	

Table 5. Properties of human body tissues

Fig. 27 presents S11 results of the folded antenna results for different position relative to the human body. Explanation of Fig. 26 is given in Table 6. From results shown in Fig. 13 we can see that the folded antenna has V.S.W.R better than 2.0:1 for air spacing up to 5mm between the antennas and patient body. If the air spacing between the sensors and the human body is increased from 0mm to 5mm the antenna resonant frequency is shifted by 5%.

Sensor position	Plot colure
Shirt thickness 0.5mm	Red
Shirt thickness 1mm	Blue
Air spacing 2mm	Pink
Air spacing 4mm	Green
Air spacing 1mm	Sky
Air spacing 5mm	Purple

Table 6. Explanation of Fig. 26

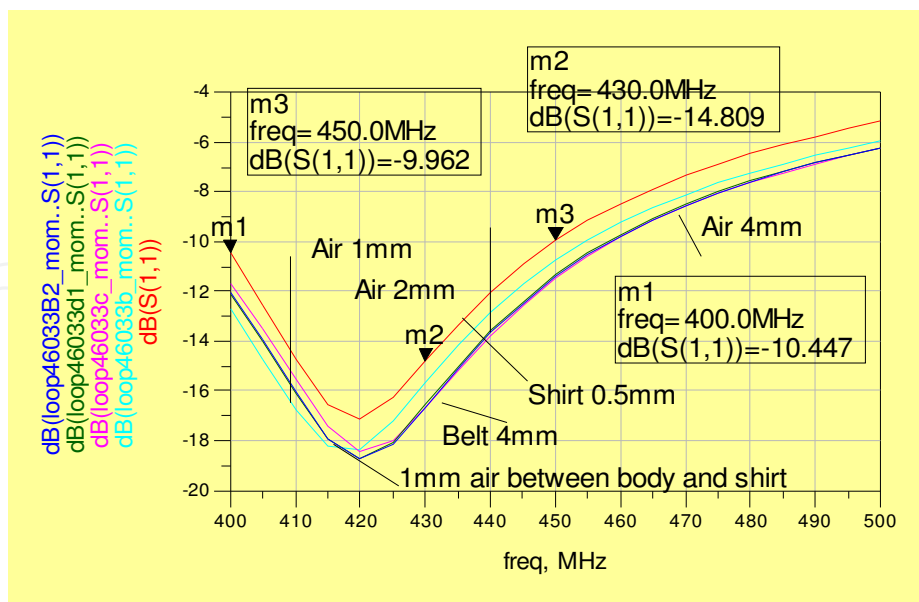| Sensor position	Colure
Shirt thickness 0.5mm	Red
Air spacing body to shirt 1mm	Blue
Belt thickness 4mm	Pink
Air spacing shirt to belt 1mm	Sky
Air spacing shirt to belt 4mm	Green

Table 7. Explanation of Fig. 27

Fig. 27. S11 results for different belt thickness

S11results in Fig. 27 presents the folded antenna matching when the belt thickness has been changed from 2 to 4mm. Explanation of Fig. 27 is given in Table 7. S11results are better than -10dB for belt thickness ranging from to 2 to 4mm. Computed S11 and S22 results was better

than-10dB for different body tissues with dielectric constant ranging from 40 to 50. Computed S11 and S22 results were better than -10dB for different shirts and belts with dielectric constant ranging from 2 to 4.

4.4 Medical applications

An application of the proposed antenna is shown in Fig. 28. Three to four folded dipole antennas may be assembled in a belt and attached to the patient stomach. The cable from each antenna is connected to a recorder. The received signal is routed to a switching matrix. The signal with the highest level is selected during the medical test. The antennas receive a signal that is transmitted from various positions in the human body. Folded antenna may be also attached on the patient back in order to improve the level of the received signal from different locations in the human body. Fig. 29 and Fig. 30 show various antenna locations on the back and front of the human body for different medical applications. In several applications the distance separating the transmitting and receiving antennas is less than $2D^2/\lambda$, where D is the largest dimension of the source of the radiation. In these applications the amplitude of the electromagnetic field close to the antenna may be quite powerful, but because of rapid fall-off with distance, they do not radiate energy to infinite distances, but instead their energies remain trapped in the region near the antenna, not drawing power from the transmitter unless they excite a receiver in the area close to the antenna. Thus, the near-fields only transfer energy to close distances from the receivers, and when they do, the result is felt as an extra power-draw in the transmitter. The receiving and transmitting antennas are magnetically coupled. Change in current flow through one wire induces a voltage across the ends of the other wire through electromagnetic induction. The amount of inductive coupling between two conductors is measured by their mutual inductance. In these applications we have to refer to the near field and not to the far field radiation pattern.
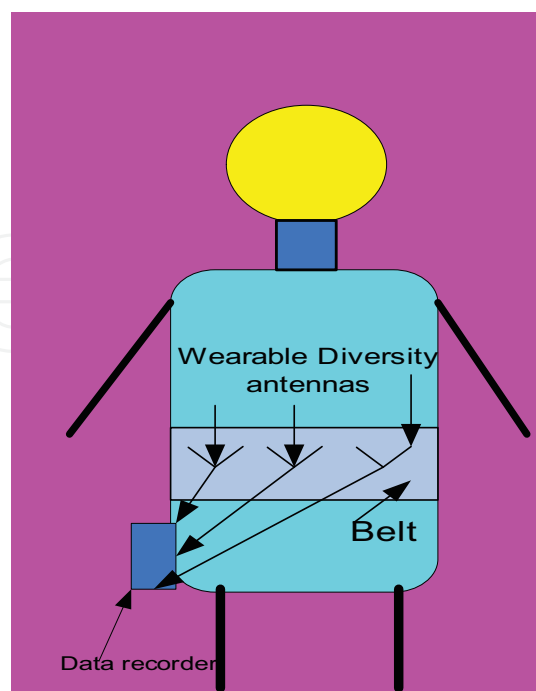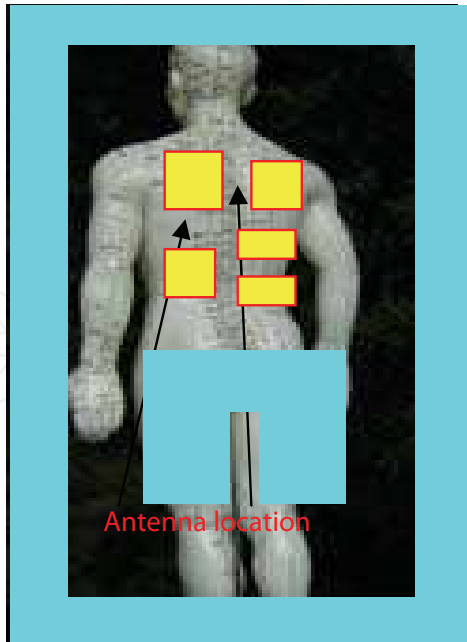

Fig. 28. Wearable antenna

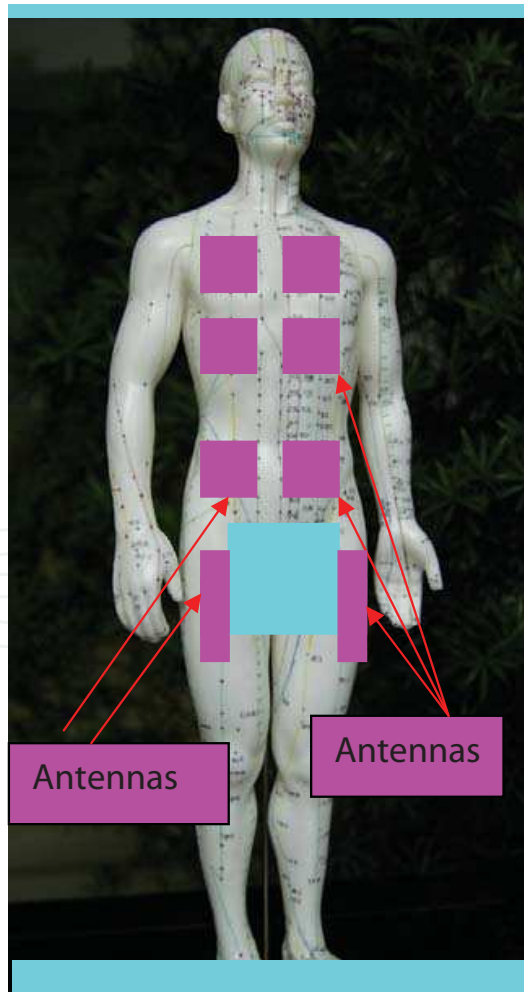Fig. 29. Printed Antenna locations on the back for medical applications

Fig. 30. Printed Patch Antenna locations for medical applications

In Fig. 31and 32 several microstrip antennas for medical applications at 434MHz are shown.
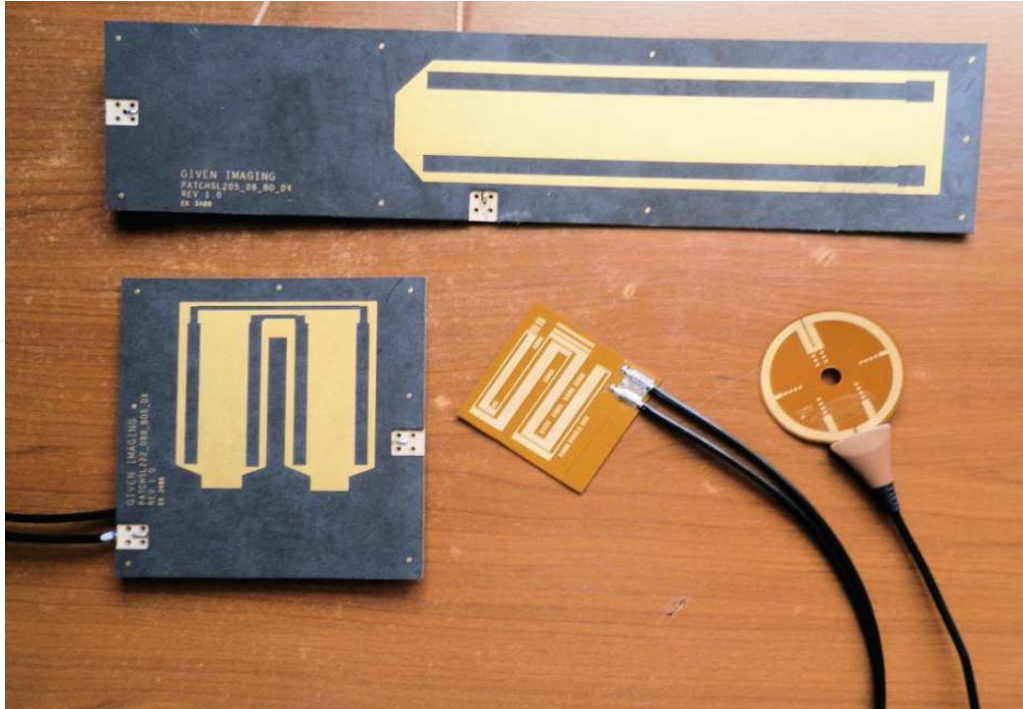

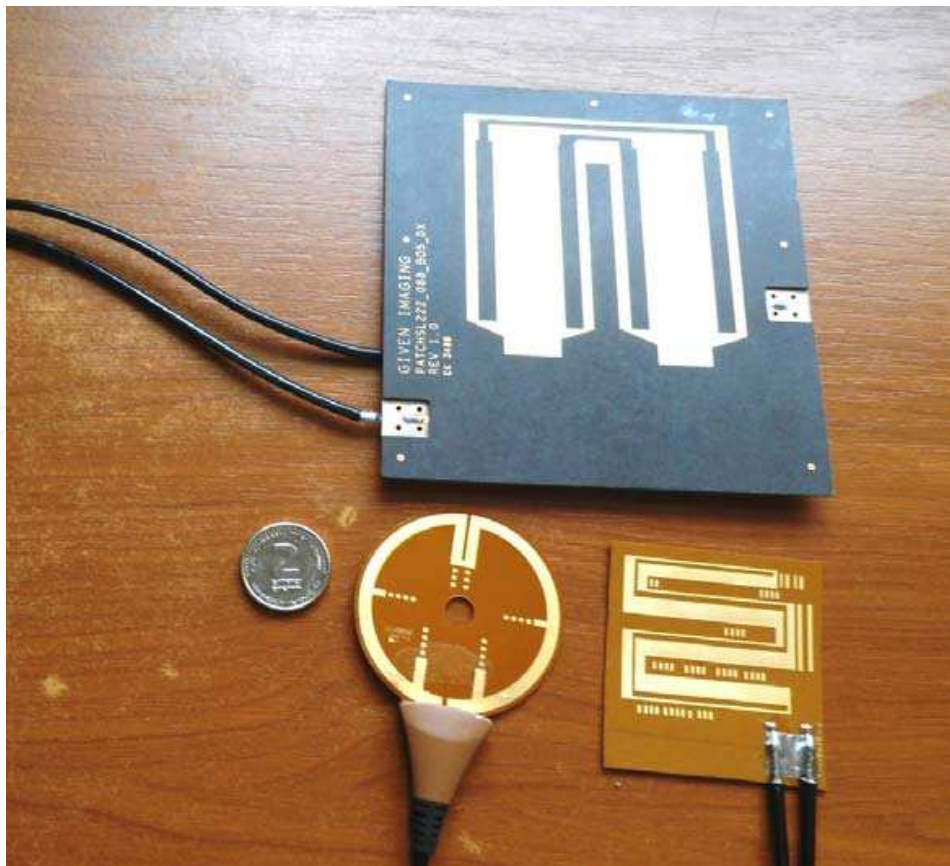
Fig. 31. Microstrip Antennas for medical applications

Fig. 32. Microstrip Antennas for medical applications

In Fig. 31 and in Fig. 32 one can see different designs of dual polarized microstrip antennas with 10% bandwidth around 434MHz. The loop antenna is with a ground plane on the antenna back. The loop antenna diameter is around 50mm.

5. Conclusion

A 64 microstrip antenna array with efficiency of 67.6% and a 256 microstrip antenna array with efficiency of 50.47% have been presented in this Chapter. Methods to reduce losses in mm-wave microstrip antenna arrays have been described in this Chapter. The results presented in this chapter point out that radiation losses need to be taken into account for accurate microstrip antenna array design at mm wave frequencies. By minimizing the number of bend discontinuities the gain of the 256 microstrip antenna array has been increased by 1dB.

Several applications of mm wave microstrip antenna arrays have been presented. Losses in the microstrip feed network form a significant limit on the possible applications of microstrip antenna arrays in mm wave frequencies. MM wave microstrip antenna arrays may be employed in communication links, seekers and detection arrays. The array may consist around 256 elements to 1024 elements. Design considerations of the antenna and the feed network are given in this chapter. Optimization of the antenna structure and feed network allows us to design and fabricate microstrip antenna arrays with high efficiency.

This chapter presents wideband microstrip antennas with high efficiency for medical applications. The antenna bandwidth is around 10% for VSWR better than 2:1. The antenna beam width is around 100°. The antenna gain is around 2dBi. The antenna S11 results for different belt thickness, shirt thickness and air spacing between the antennas and human body are given in this chapter. The effect of the antenna location on the human body should be considered in the antenna design process. If the air spacing between the sensors and the human body is increased from 0mm to 5mm the antenna resonant frequency is shifted by 5%.The proposed antenna may be employed in Medicare RF systems.

6. References

J.R. James, P.S Hall & C. Wood, (1981). Microstrip Antenna Theory and Design,1981.

A. Sabban & K.C. Gupta, (1991). Characterization of Radiation Loss from Microstrip Discontinuities Using a Multiport Network Modeling Approach, I.E.E.E Trans. on M.T.T, Vol. 39,No. 4, April 1991,pp. 705-712.

A. Sabban, (1991). PhD Thesis, Multiport Network Model for Evaluating Radiation Loss and Coupling Among Discontinuities in Microstrip Circuits, University of Colorado at Boulder, January 1991.

P.B. Kathei & N.G. Alexopoulos, (1985). Frequency-dependent characteristic of microstrip, MTT-33, discontinuities in millimeter-wave integrated circuits, IEEE Trans. Microwave Theory Tech, vol. pp. 1029-1035, Oct. 1985.

A. Sabban, (1983). A New Wideband Stacked Microstrip Antenna, I.E.E.E Antenna and Propagation Symposium, Houston, Texas, U.S.A, June 1983.

A. Sabban & E. Navon (1983). A MM-Waves Microstrip Antenna Array, I.E.E.E Symposium, Tel-Aviv, March 1983.

A. Sabban, (1981). Wideband Microstrip Antenna Arrays, I.E.E.E Antenna and Propagation Symposium MELCOM, Tel-Aviv,1981.

M. M. Milkov, (2000). Millimeter-Wave Imaging System Based on Antenna-Coupled Bolometer, MSc. Thesis, UCLA UCLA (2000).

G. de Lange et. al., (1999). A 3*3 mm-wave micro machined imaging array with sis mixers, Appl. Phys. Lett. 75 (6), pp. 868-870 (1999).

A. Rahman et. al., (1996). Micromachined room temperature microbolometers for mm-wave detection, Appl. Phys. Lett. 68 (14), pp. 2020-2022 (1996).

A. Luukanen et. al., US Patent 6242740 (2001).

M. D. Jack et. al., (2001). US Patent 6329655 (2001).

G. N. Sinclair et. al., (2000). Passive millimeter wave imaging in security scanning, Proc. SPIE Vol. 4032, pp. 40-45, (2000).

G. Kompa & R. Mehran, (1975). Planar waveguide model for computing microstrip components, Electron Lett., vol. 11, no. 9, pp. 459-460, 1975.

Lawrence C. Chirwa; Paul A. Hammond; Scott Roy & David R. S. Cumming, (2003). Electromagnetic Radiation from Ingested Sources in the Human Intestine between 150 MHz and 1.2 GHz, IEEE Transaction on Biomedical eng., VOL. 50, NO. 4, pp. 484-492, April 2003.

D.Werber; A. Schwentner & E. M. Biebl, (2006). Investigation of RF transmission properties of human tissues, Adv. Radio Sci., 4, pp. 357–360, 2006.
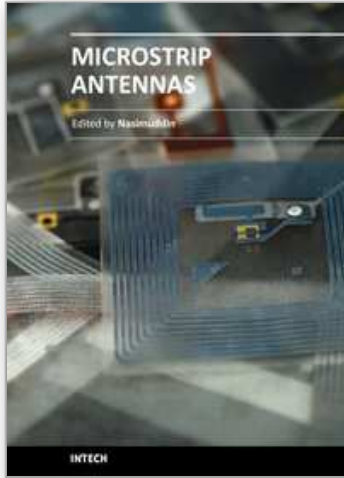
Microstrip Antennas

Edited by Prof. Nasimuddin Nasimuddin

In the last 40 years, the microstrip antenna has been developed for many communication systems such as radars, sensors, wireless, satellite, broadcasting, ultra-wideband, radio frequency identifications (RFIDs), reader devices etc. The progress in modern wireless communication systems has dramatically increased the demand for microstrip antennas. In this book some recent advances in microstrip antennas are presented.

How to reference

In order to correctly reference this scholarly work, feel free to copy and paste the following:

INTECH
open science | open minds